行政院國家科學委員會專題研究計畫 成果報告

應用具有嵌入式主動視覺無線網路系統於自走車之研究(第2年)
研究成果報告(完整版)

計 畫 類 別 ：個別型
計 畫 編 號 ：NSC 96-2221-E-032-012-MY2
執 行 期 間 ：97年08月01日至98年07月31日
執 行 單 位 ：淡江大學電機工程學系

計 畫 主 持 人：黃志良

計畫參與人員：碩士班研究生-兼任助理人員：李昇遠

報 告 附 件 ：出席國際會議研究心得報告及發表論文

處 理 方 式 ：本計畫可公開查詢

中 華 民 國 98年09月04日

行政院國家科學委員會補助專題研究計畫成果報告

應用具有嵌入式主動視覺無線網路系統於自走車之研究(2/2)

計畫類別：■ 個別型計畫　　□ 整合型計畫
計畫編號：NSC 96-2221-E-032-012-MY2
執行期間：：97 年 8 月 1 日至 98 年 7 月 31 日

計畫主持人：黃志良
共同主持人：
計畫參與人員：許庭嘉、傅建鈞、李昇遠

成果報告類型(依經費核定清單規定繳交)：□精簡報告　■完整報告

本成果報告包括以下應繳交之附件：
□赴國外出差或研習心得報告一份
□赴大陸地區出差或研習心得報告一份
□出席國際學術會議心得報告及發表之論文各一份
□國際合作研究計畫國外研究報告書一份

處理方式：除產學合作研究計畫、提升產業技術及人才培育研究計畫、列管計畫及下列情形者外，得立即公開查詢
□涉及專利或其他智慧財產權，□一年□二年後可公開查詢

執行單位：淡江大學電機工程學系

中　　華　　民　　國 98 年 9 月 4 日

應用具有嵌入式主動視覺無線網路系統於自走車之研究(2/2)

計畫編號：NSC-96-2221-E-032-012-MY2

執行期間：97 年 8 月 1 日至 98 年 7 月 31 日

主　持　人：黃志良　淡江大學電機工程學系

計畫參與人員：許庭嘉、傅建鈞、李昇遠　淡江大學電機工程學系

中文摘要

本計畫乃是應用主動嵌入式視覺系統(Active Embedded Vision System (AEVS))及差速機器人(Differential Mobile Robot(DMR))來實現分佈的主動嵌入視覺網路系統中差速機器人包括折線軌跡追蹤及躲避障礙之導引。所應用的AEVS包括數位訊號處理器(TMS320DM642EVM)及具高速迴轉台之攝影機(Speed Dome)。而DMR包括兩組直流馬達、一個微處理器TMS320F2812、一個驅動電路和一個無線模組，其具有零迴轉半徑，更適合於折線軌跡追蹤。由於TMS320DM642內定的彩色影像輸出格式為YCrCb，故將紅色和矩形特徵貼於DMR上，而藍色和圓形特徵貼於障礙物上，以利於其辨識及定位。接著由迴轉台所捕捉到的影像訊號輸入到TMS320DM642，以進行如下的影像處理：分割紅色或藍色、二值化、以中值濾波器去除雜訊、計算面積、求中心位置的座標，然後以多層感知器類神經網路建立影像平面座標與世界座標的轉換。所謂的分佈的AEVS (Distributed AEVS(DAVES))，即是應用至少兩組AVES於適當的位置監控相關空間內的DMR，並追蹤因建築物限制所規劃的折線軌跡及躲避相關障礙，以解決典型的輪型機器人所遭遇的定位、軌跡追蹤及躲避障礙之問題。一般的分佈式視覺系統都是固定的，它們監控區域是有限的，如果要增加監控的區域則須要增加攝影機的數量，如此一來，會導致系統更加地複雜。雖然全方位的視覺系統可觀看360度的區域，由於其具有很大影像失真，它的影像處理須要消耗大量的計算時間和它的估測(或校正)誤差亦很大。因此我們將應用模糊可變結構控制(Fuzzy Decentralized Variable Structure Control (FDVSC))，驅動AEVS以鎖住運動中的DMR，並以FDVSC操控DMR進行折線軌跡追蹤及躲避障礙。最後以相關實驗，驗證所建議系統的優越性及有效性。

關鍵詞：分佈式的主動嵌入視覺網路空間、差速機器人、導航、折線軌跡追蹤及躲避障礙、模糊可變結構控制、多處理器控制系統。

Abstract --- The trajectory tracking and obstacle avoidance of a differential mobile robot (DMR) in a distributed active embedded vision system (DAEVS) is developed. The proposed active embedded vision system (AEVS) includes the digital signal processor (DSP) and the speed dome with the vision of high-speed feature. For the purpose of easy recognition and localization of DMR and obstacle, the red and rectangular shape and the blue and circle shape are respectively placed on the top of the DMR and the obstacle. In the beginning, the visual information coming from the speed dome is transferred to the DSP to execute the corresponding image processing: the segmentation of red or blue component, the binary processing, the removal of noise by median filter and shape feature, and the calculation of the area and central position of image feature. Because the task is planned in the world coordinate and because the relation between the image plane coordinate and the world coordinate is highly nonlinear, a multilayer neural network (MNN) is employed to establish the relation between them. From the viewpoint of the constraint of house architecture, the energy consumption of DMR, and the ease of path planning, a desired trajectory made up by a set of piecewise lines is addressed. Simultaneously, three trajectory tracking modes: approach mode, fine-tune mode, and inertia-navigation mode, are designed to obtain a fast trajectory tracking with the energy saving manner. Finally, the corresponding experiments of the trajectory tracking and obstacle avoidance for a DMR in the DAEVS confirm the validity and efficiency of the proposed methodology.

Keywords: Distributed active embedded vision system, Differential mobile robot, Navigation, Trajectory tracking, Obstacle avoidance, Fuzzy decentralized variable structure control.

I. Introduction

Recently, distributed control within sensor networks has received wide attention in many engineering applications. Some representative works may be found in [1]-[9]. The distributed network-space system can monitor the occurrence within itself, build its own models, communicate with its inhabitants, and act on the decisions made by itself. For instance, a mobile robot is designed to track a trajectory, which is often made up by a set of piecewise lines from the viewpoint of the constraint of house architecture, the energy consumption of mobile robot, and the ease of path planning [9]. Simultaneously, the obstacle avoidance is accomplished. In addition, many problems encountered in classic mobile robots (e.g., localization [10], [11], high computational power [12], [13], different software for different kinds of mobile robot [14], interference between sensors [15]) may be resolved when they are cast into a distributed vision system.

On the other hand, almost all distributed visions are fixed. Therefore the visible region is limited or the number of visions must be increased when the monitored area is increased ([2]-[5]). Although the omni-directional vision system (ODVS) possesses a 360° view angle, its image processing is time-consuming and the estimation error (or modeling error) is large owing to the image

distortion [1], [16], [17]. In this project, each AEVS contains a digital signal processor (DSP, e.g., TMS320DM642 from Texa Instrument Co.), a speed dome with the vision of high-speed feature, and a wireless device. The proposed AEVS possesses the function of image processing, the calculation of the control law to drive the vision system, the communication among AEVSs and DMRs. To obtain an easy recognition and localization of DMR and obstacle, the red and rectangular shape and the blue and circle shape are respectively placed on the top of the DMR and the obstacle. First, the visual information coming from the speed dome is transferred to the TMS320DM642 DSP to execute the corresponding image processing: the segmentation of the red and rectangular landmark or the blue and circular landmark, the image binary processing, the removal of noise by median filter and shape feature, and the calculation of the area and central position of image landmark. Because the task is planned in the world coordinate and because the relation between the image plane coordinate and the world coordinate is highly nonlinear, a multilayer neural network is also employed to establish the relation between them. In summary, the first difference as compared with the previous studies (e.g., [8], [9]) is an active embedded vision system, possessing portable, computational, and wireless features are more suitable for the distributed sensor network system. Under these circumstances, the DAEVS with the real-time posture estimation of a DMR can augment the visible area, can simultaneously reduce the time for image processing, and can obtain an accurate modeling between the image plane coordinate and the world coordinate [18], [19].

It is known that the manipulation of a DMR is different from that of a car-like mobile robot (CLMR) [8], [9], [15], [20] which can control its orientation by the front wheel and control its translation velocity by the rear wheel. Therefore, the manipulation of a DMR must be addressed. After the image processing is completed, the estimated posture of the DMR or obstacle is employed to accomplish the assigned task. First, the desired angular position and translation velocity for specific task are obtained. Then the corresponding desired angular velocities of the right and left wheels for specific task are derived by the kinematics of a DMR. Thus the fuzzy decentralized variable structure control algorithm (e.g., [9]) realized in the TMS320F2812 DSP of the DMR is employed to respectively drive the velocities of the right and left wheels to reach the desired values [20]. In addition, the operation of a DMR does not have the minimum turning radius as compared with a CLMR [8], [9], [15], [20]. It is then expected that the tracking response of the piecewise-lines trajectory with (or without) the obstacle avoidance for a DMR in the DAEVS is much better than that of a CLMR. This is the second difference as compared with the previous studies (e.g., [8], [9], [15], [20]). From the viewpoint of the constraint of house architecture, the energy consumption of DMR, and the ease of path planning, a desired trajectory made up by a set of piecewise lines is also considered in this project. The strategy for the trajectory tracking is designed and includes the following three modes: (i) approach mode, (ii) fine-tune mode, and (iii) inertia-navigation mode. This is the third difference as compared with the previous papers. Finally, the corresponding experiments of trajectory tracking and obstacle avoidance are arranged to confirm the effectiveness of the proposed control system.

The outline of this project is described as follows. In the next section, system description and research task are given. In section 3, an image processing and a modeling using MNN are introduced. In section 4, the manipulation of a DMR is designed to obtain the assigned task. Then the result of posture estimation, the strategy for tracking a segment of trajectory, and the search of DMR or obstacle, are introduced in the experimental preliminaries of section 5. Experimental results of trajectory tracking and obstacle avoidance are also presented in this section. Finally, the conclusions are arranged in section 6.

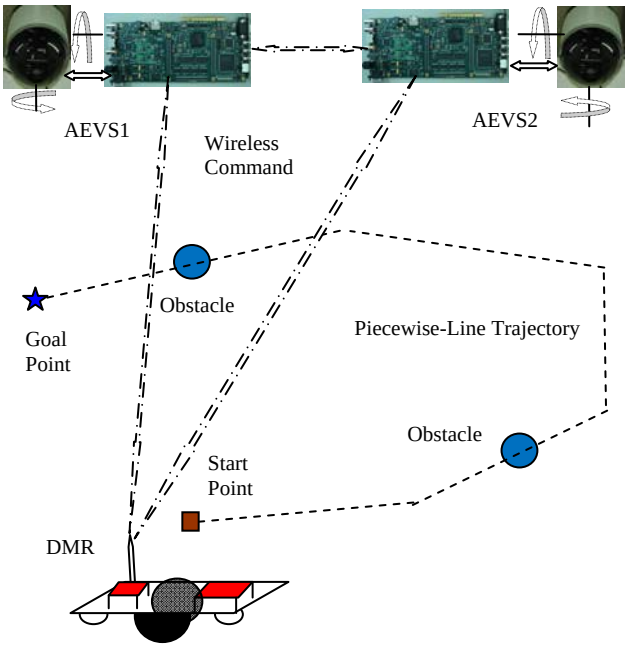

Fig. 1. The diagram of the overall control system.

II. System Description and Research Task

2.1 System Description

Figure 1 shows the experimental setup of a DMR in the DAEVS. The overall control system includes a DMR, and two AEVSs. A DMR includes two DC motors with driver, one microprocessor of TMS320F2812, and a wireless device. Each AEVS contains the digital signal processor TMS320DM642 from Texa Instrument Co., the speed dome with the vision of high-speed feature, and a wireless device. The important specifications of this DSP are described as follows: two channel for analog signal of vision with the format of NTSC or PAL, two VGA outputs, two RS232 communication ports, 10/100mMbps Ethernet, stereo and digital audio input/output ports, 4MB Flash memory, 32MB SDRAM, PCI interface, and 720MHz clock speed. The specifications of the DMR are given in Table 1. The specification of the speed dome with the vision of high-speed feature are described as follows: RS485 communication port, analog signal of vision with the

format NTSC, power consumption 13W, minimum illumination 0.3Lux, horizontal resolution 480 TV lines, and signal/noise over 50dB. It is also known that the bandwidths of the proposed AEVS1 and 2 are much larger than that of the DMR. In brief, the first difference as compared with the previous studies (e.g., [8], [9]) is an active embedded vision system, possessing portable, computational, and wireless features are more suitable for the distributed sensor network system.

Two rectangular landmarks with red color and different size are used on the DMR (see Fig. 2). The microprocessor in DMR is the TMS320F2812 from TI Co. with the following important specifications: two event managers (i.e., EVA and EVB), series communication interface (SCI), series periphery interface (SPI), enhanced control array network (eCAN), multi-channel buffer series peripheral (McBSP), analog to digital conversion (ADC), 128KB Flash memory, 18KB SARAM, and 150MHz clock speed [21]. It is known that almost no minimum turning radius for a DMR occurs [11]. The trajectory tracking for a set of piecewise-lines with (or without) obstacle avoidance is much better than that of the CLMR. This feature will be confirmed by the experiments. This is the second difference as compared with our previous study [9].

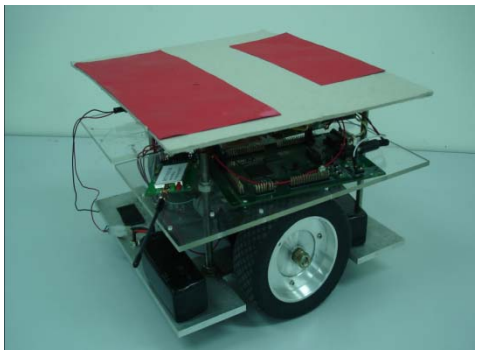

Fig. 2. Photograph of the DMR with two rectangular landmarks of red color and different size.

Table 1. The specifications of DMR.

Specification	Quantity
Length	320 mm
Width	280 mm
Height	200mm
Weight	4.9kg
Radius of Wheel	125 mm
Distance Between Wheels	240 mm

2.2 Research Task

In the beginning, two DC servo motors for the left and right wheels are controlled by individual fuzzy variable structure (FVSC). Hence, the proposed control is called fuzzy decentralized variable structure control (FDVSC). The details can be found from the previous papers, e.g., [9]. As one knows, the manipulation of a DMR is different from that of a CLMR. Hence, an effective operation of a DMR will be introduced to obtain the desired task. In addition, the strategy for the navigation of a DMR to the trajectory of piecewise-lines includes the following three modes: (1) approach mode, (2) fine-tune mode, (3) inertia-navigation mode. This is the third difference as compared with the previous papers. Similarly, two sets of FDVSCs for the AEVS1 and 2 can be effectively implemented to lock the DMR into the center of visual window once it is inside of visual window.

The main goal of this project is to investigate the trajectory tracking with (or without) obstacle avoidance using three sets FDVSCs for a DMR in a DAEVS with two AEVSs. The experiment is performed for four cases: (i) with initial lock of the DMR in the DAEVS, the trajectory tracking of a set of piecewise-lines with the reference command of translation velocity 35*cm/s*; (ii) the requirement of a search to lock the DMR for the same trajectory of part (i); (iii) the tracking of the same trajectory of part (i) with one or two static obstacles; and (iv) the same experiment of part (iii) with different lighting condition.

III. Image Processing and Neural Network Modeling

3.1 Image Processing

The background of the DAEVS (i.e., the ground in Fig. 3(a) contains similar size pattern as compared with DMR, some lines in the ground, and non-uniform illumination) is difficult to deal with [22]-[24]. The following six-step procedure shows how to obtain the position error of the DMR with respect to the image center. The position error is then used to lock the image of the DMR into the center of the lens such that the distortion of lens is reduced [25].

A. Image acquisition

The speed dome is the vision sensor to obtain the information of color image which is then transmitted to the DSP-TMS320DM642 having 720×480 pixels. To increase the processing speed, the grabbed color image is compressed into 360×240 pixels. Because the default format of the TMS320DM642 is YC_rC_b $4:2:2$, where Y represents the luminance component, and C_r , C_b are respectively chrominance components of red and blue, no conversion of color space is required.

B. Image segmentation

Since the value of Y is strongly dependent on the luminance, it will not be considered in this project. The ranges of the C_r and C_b for the DMR and the obstacle are different. Together with the shape feature (i.e., rectangle and circle), the process of the image segmentation is more robust in distinguishing the DMR and the obstacle from the ground.

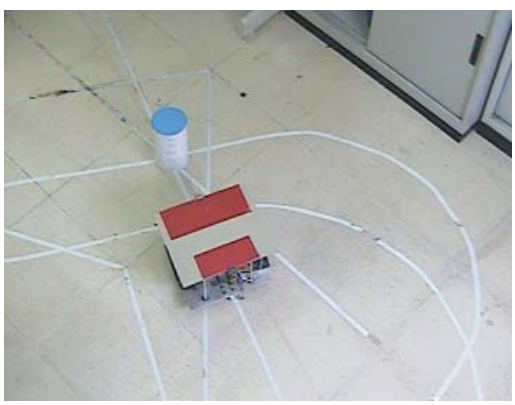

(a) Source image.

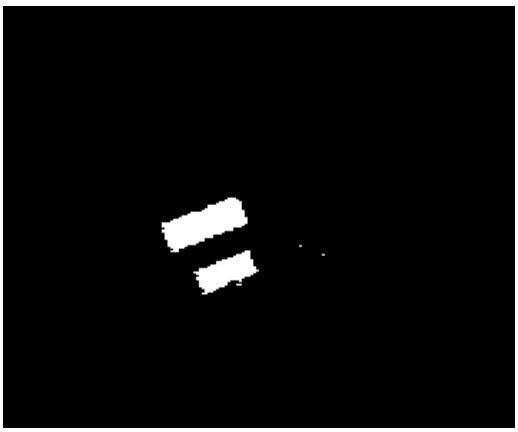

(b)Binary image for the red DMR.

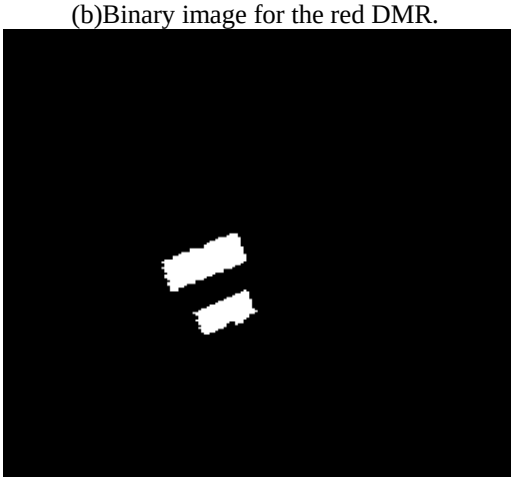

(c) Median filtering for the red DMR.

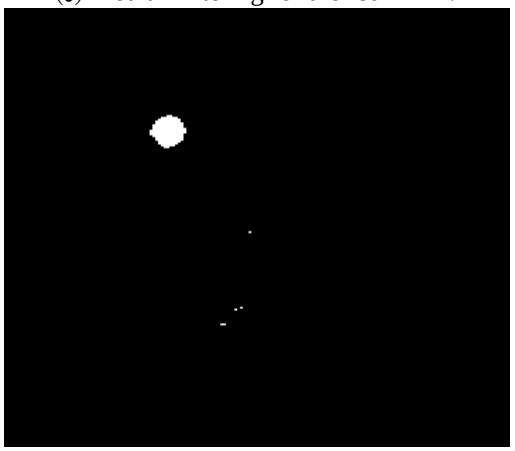

(d) Binary image for the blue obstacle.

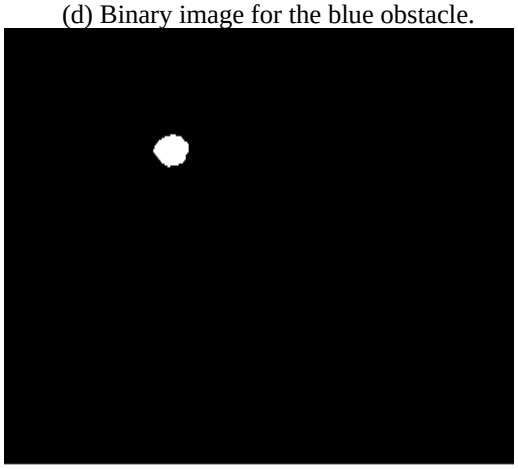

(e) Median filtering for the blue obstacle.

Fig. 3. The result of the image processing.

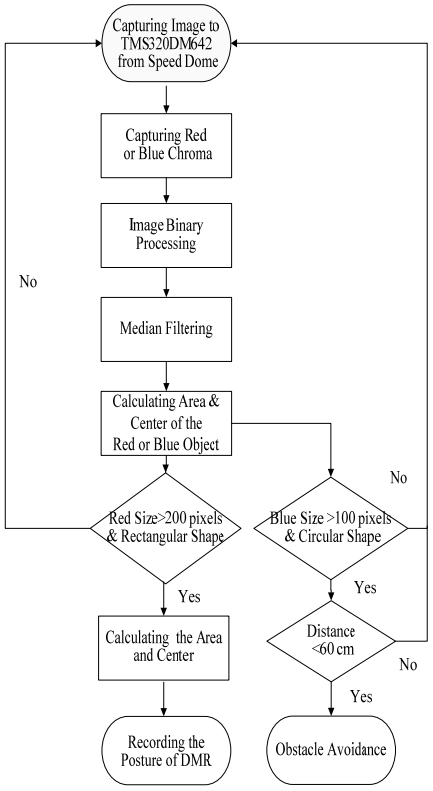

Fig. 4. Flow chart of the image processing.

C. Binary

In this project, a double thresholding technique is applied to the component of C_r and C_b such that a binary image is obtained. The corresponding relation is

$$D(I_x, I_y) = \begin{cases} 1, & \text{if } T_{b2} \geq f(I_x, I_y) \geq T_{b1} \\ 0, & \text{otherwise} \end{cases} \quad (1)$$

where $f(I_x, I_y)$ denotes the values of C_r and C_b on the image plane (I_x, I_y), $D(I_x, I_y) = 1$ stands for the white pixels, and $D(I_x, I_y) = 0$ stands for the black pixels. The purpose of binary is to reduce the storage amount as well as the computation load. The values of T_{b1} and T_{b2} are less sensitive to lighting conditions because the *Y* component is not considered for the binary operation. After tests, the suitable ranges of C_r and C_b for the DMR and the obstacle are respectively $C_r \in [140,180]$, $C_b \in [240,255]$, and $C_r \in [160,250], C_b \in [120,160]$.

D. Shape feature

To increase the robustness of and simplify the image processing, the rectangular and circular shapes respectively representative the DMR and obstacle are considered.

$$R_{shape} = 4\pi A / L^2 \quad (2)$$

where A and L are respectively the area and circumference of the specific landmark. For an exact circular landmark, $R_{shape} = 1;$ for the rectangular landmarks with width/length 1:3 and 1:2, $R_{shape} = 3\pi/16$ and $R_{shape} = 2\pi/9$, respectively.

E. Image reconstruction

After the aforementioned preprocessing (i.e., parts *A*~*D*), there may be some white salts or black peppers and disconnections of edge. In this case, the image reconstruction using median filter is employed to eliminate the disturbances caused by preprocessing (see Figs. 3(c) and (e)).

F. Image representation and description

The area, center, and coordinate of image features are considered to represent the posture of the DMR on the image plane coordinate. For digital image, their 2D moments of order $p+q$ and centered moments are defined as follows [22]-[23], [25]:

$$m_{pq} = \sum_{I_x} \sum_{I_y} I_x^p I_y^q f(I_x, I_y) \tag{3}$$

$$\mu_{pq} = \sum_{I_x} \sum_{I_y} \left(I_x - \bar{I}_x\right)^p \left(I_y - \bar{I}_y\right)^q f(I_x, I_y) \tag{4}$$

where $f(I_x, I_y)$ is the same as (1), $p, q \geq 0$, and $\bar{I}_x = \sum_{(I_x, I_y)\in\Omega} \sum I_x / N$, $\bar{I}_y = \sum_{(I_x, I_y)\in\Omega} \sum I_y / N$ denotes the center of the area N of the desired image feature Ω. The areas and centers of the image features 1 and 2 in Fig. 5 can be calculated by (3) and (4) respectively. The central position (I_{Rx}, I_{Ry}) and orientation θ_I (i.e., posture) of the DMR on the image plane can then be computed as

$$\left(I_{Rx}, I_{Ry}\right) = \left\{\left(I_{Rx}^1, I_{Ry}^1\right) + \left(I_{Rx}^2, I_{Ry}^2\right)\right\} / 2,$$

$$\theta_I = \tan^{-1}\left\{\left(I_{Ry}^2 - I_{Ry}^1\right) / \left(I_{Rx}^2 - I_{Rx}^1\right)\right\}. \tag{5}$$

In this project, the height of the obstacle is assumed to be the same as that of the DMR. Then, the centers and areas of obstacles can be estimated using the same learned weight and bias values for the DMR.

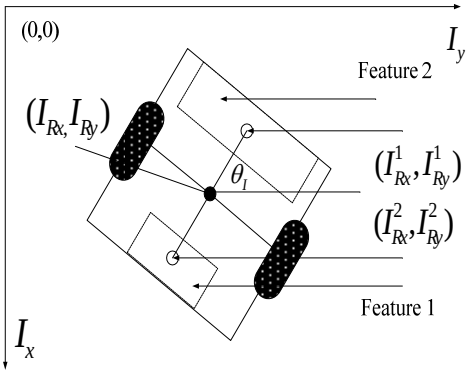

Fig. 5. Illustration of the image features and calculation of the posture of the DMR on the image plane.

3.2 Neural Network Modeling

Generally, a homogeneous coordinate is employed to establish a camera model; however, this method needs accurate calibration and is therefore impractical. In addition, different mechanisms for driving the pan and tilt motion will result in different kinematic and dynamic relationships. Under these circumstances, an effective method using multilayer neural network (MNN) is applied to model the relation between the world coordinate and the image plane coordinate. From Fig. 6, different visible areas are obtained for different angles of the tilt and pan motion; e.g., the area denoted by the dash-dot line is for $\theta_x = 0^\circ$, $\theta_y = 45^\circ$, and the area denoted by the solid line is for $\theta_x = -22.5^\circ$, $\theta_y = 37.5^\circ$. We note that these relations are highly nonlinear [18], [19], [22]-[25]. This motivates the use of MNN for modeling. The advantage of this method is that a camera model and the kinematic and dynamic relations of mechanism are not required.

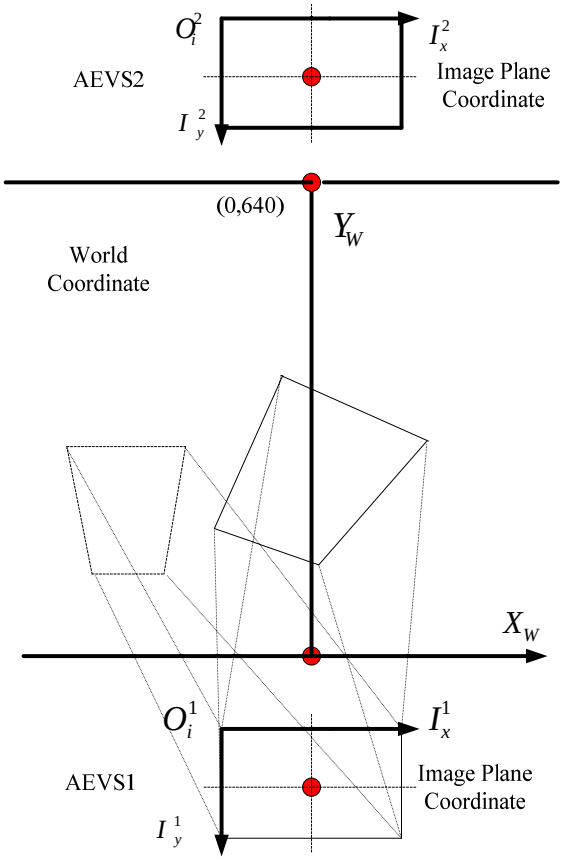

Fig. 6. Modeling between the image plane coordinate and the world coordinate.

B. Multilayer neural network

A three-layer MNN, including input-layer, hidden-layer, and output-layer, is depicted in Fig. 8. The inputs of the MNN are the angles of the pan-tilt platform and the position of the DMR on the image plane coordinate respectively given as $\theta_x, \theta_y, I_{Rx}$, and I_{Ry}. The outputs are the position of the DMR on the world coordinate given as X_{Rw} and Y_{Rw}. To avoid the complexity of the MNN, the orientation of the DMR is not set as its output. It is indirectly calculated by (4) because the orientation is only used for the navigation of direction. The following "cost" is assigned for deriving the learning law:

$$\varepsilon = \sum_{k=1}^{2} (d_k - y_k)^2 / 2 \tag{6}$$

where d_k is the desired output (or target), and y_k is the output of MNN. Figure 7 shows the concept for the different postures of the DMR monitored by the same angles of AEVS1 or 2 (e.g., the area enclosed by the solid line). The data in this region should have the representative relationship between the world coordinate and the image plane coordinate. Similarly, the data for different postures of the AEVS1 or 2 are obtained. After using $\left\{\left(x_i(n), y_k(n)\right)\right\}$, where $i = 1,2,3,4, k = 1,2$, and $n = 1,2,..,M$, with M being the total pair of data, these

data are fed into the MNN with the generalized back propagation learning algorithm, e.g., Conjugate Gradient algorithm, Levenberg-Marquart algorithm. The proposed architecture of MNN is shown in Fig. 8 with $\mathrm{P}=\left[\theta_x\ \theta_y\ I_{Rx}\ I_{Ry}\right]^T$, $\mathrm{a}^2=\left[x_{Rw}\ y_{Rw}\right]^T$, $f_i^1(n_i^1)=\left(1-e^{-n_i^1}\right)\Big/\left(1+e^{-n_i^1}\right)$, $i=1,2,...,29$, and $f_j^2(n_j^2)=n_j^2$, $j=1,2$. The upper subscript of Fig. 8 denotes the corresponding number of the layer, the symbols f_i^k and n_i^k are the *ith* component of the vectors $\mathbf{f}^k$ and $\mathbf{n}^k$, $k=1,2$.

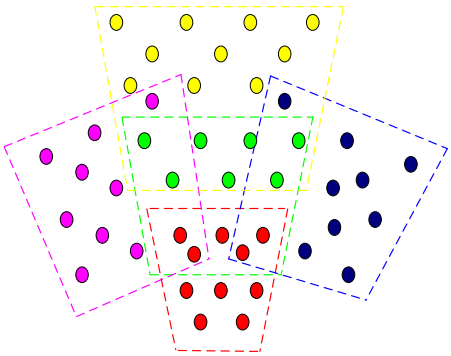

Fig. 7. Acquisition of the representative training data for MNN.

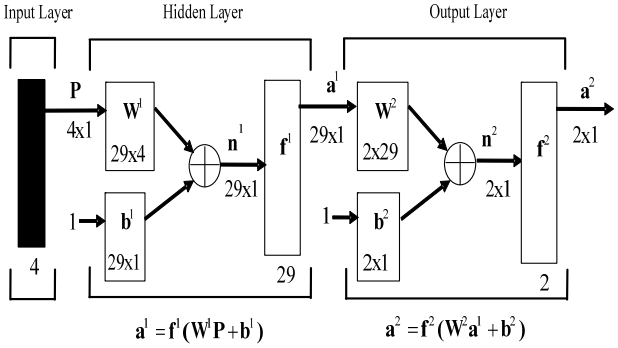

Fig. 8. Modeling via MNN.

The software of MATLAB can help to train the weight and bias values of the MNN. The inputs of the proposed MNN are respectively normalized by $\pi/180$, $\pi/180, 1/180$, and $1/180$. Similarly, the normalizations of the output signal are all assigned as 500. Figure 9 shows the flow chart for the modeling of MNN. After an effective modeling via MNN (refer to Figs. 10 and 11), the transform between the image plane coordinate and the world coordinate is achieved. Figure 10 shows the convergence of learning process is fast. The symbols of star in Figs. 11(a) and (b) represent the targets (or desired output) of MNN to be approximated. The corresponding modeling errors in Figs. 11 (c) and (d) are good enough.

A mobile robot using an omni-directional vision system (ODVS) possesses 360° view angle [1], [16], [17]. No servo for the ODVS is needed when the monitoring region increases. Due to the distortion of the image using ODVS, its image processing is time-consuming and the estimation error is larger than the proposed method. For example, some experiments for self-localization have the average calibration error of around 30*cm* [1], [16], [17]. On the other hand, the calibration using the proposed method possesses an average calibration error of only 2*cm*. In summary, the modeling by the proposed DAEVS is much more precise and effective than that given by an ODVS.

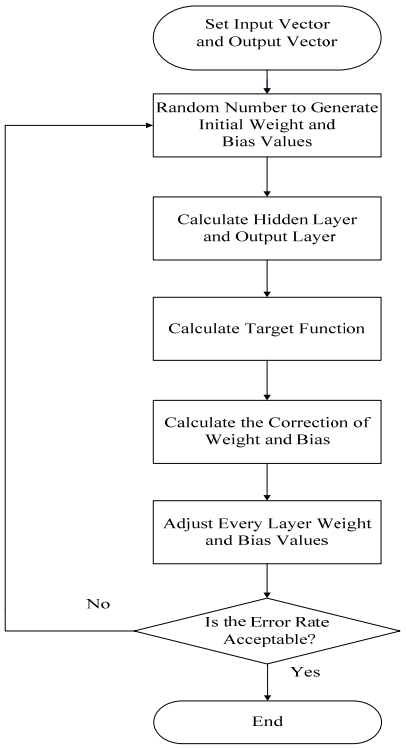

Fig. 9. Flow chart for the modeling of MNN.

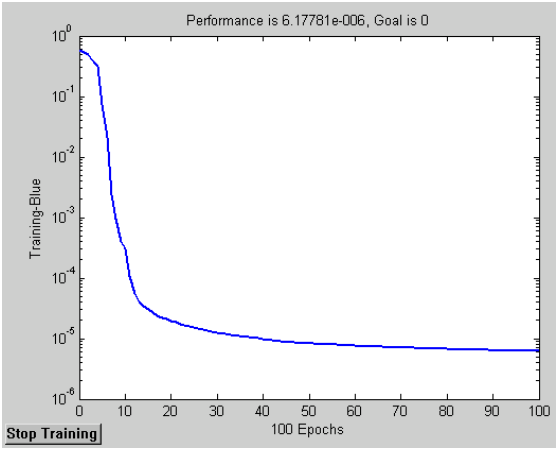

Fig. 10. Performance of learning iterations.

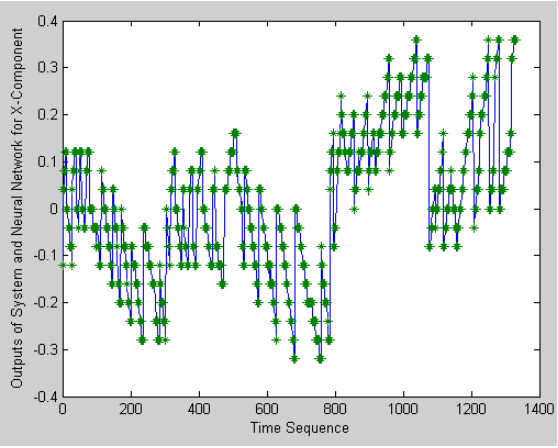

(a)

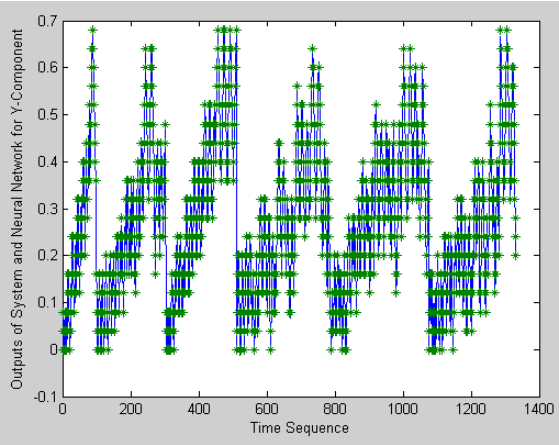

(b)

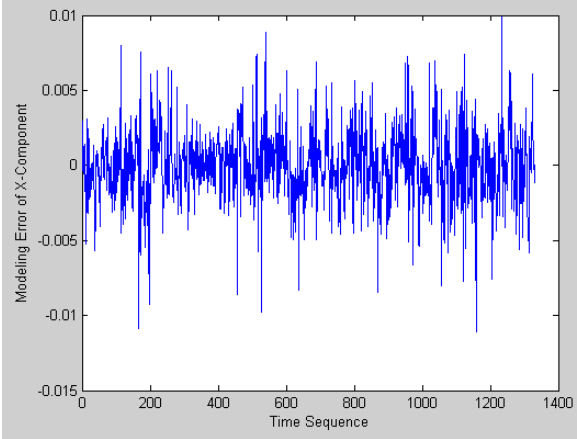

(c)

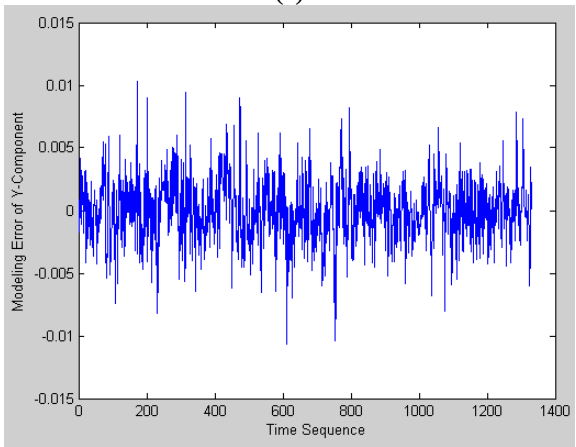

(d)

Fig. 11. Model verification of MNN.

VI. Manipulation of DMR

The manipulation of a DMR is different from that of a CLMR (e.g., [8], [9], [15], [20]), which can control the orientation by its front wheel and the translation velocity by its rear wheel. Therefore, the manipulation of a DMR must be considered. In the beginning, the kinematics of a DMR is described as follows:

$$\dot{x}(t) = v(t)\cos(\theta), \dot{y}(t) = v(t)\sin(\theta), \dot{\theta}(t) = \omega(t) \quad (7)$$

$$v(t) = \left[\omega_r(t) + \omega_l(t)\right] r/2, \omega(t) = \left[\omega_r(t) - \omega_l(t)\right] r/d \quad (8)$$

where $\theta(t)$ and $\omega(t)$ respectively denote the angular position and angular velocity with respect to z-axis, $\omega_r(t)$ and $\omega_l(t)$ are respectively the angular velocities of the right and left wheels, r is the radius of the wheel, d is the distance between two wheels. It is assumed that $\omega_r(t)$ and $\omega_l(t)$ are approximately constant in the sampling interval $\Delta t = t_k - t_{k-1}$. Then the position and orientation of a DMR are described as follows:

$$x(t_k) = x(t_{k-1}) + \bar{v}(t_k)\Delta t \cos(\theta(t_k) + \Delta\theta(t_k)) \cdot \sin(\Delta\theta(t_k))/\Delta\theta(t_k) \quad (9)$$

$$y(t_k) = y(t_{k-1}) + \bar{v}(t_k)\Delta t \sin(\theta(t_k) + \Delta\theta(t_k)) \cdot \sin(\Delta\theta(t_k))/\Delta\theta(t_k) \quad (10)$$

$$\theta(t_k) = \theta(t_{k-1}) + \bar{\omega}(t_k)\Delta t \quad (11)$$

where

$$\Delta\theta(t_k) = \bar{\omega}(t_k)\Delta t/2$$
$$\bar{v}(t_k)\Delta t = \left[\Delta q_r(t_k) + \Delta q_l(t_k)\right] r/2,$$
$$\bar{\omega}(t_k)\Delta t = \left[\Delta q_r(t_k) - \Delta q_l(t_k)\right] r/d \quad (12)$$

where $\Delta q_r(t_k)$ and $\Delta q_l(t_k)$ are respectively denoted as the angular positions of the right and left wheels for the time interval Δt. Based on the requirement of task, the corresponding path can be planned by $\theta_d(t_k)$ and $v_d(t_k)$, which respectively represent the desired angular position and translation velocity at the sampling time t_k. Then the corresponding angular velocity can be expressed as $\omega_d(t_k) = \left[\theta_d(t_k) - \theta(t_{k-1})\right]/\Delta t$. Finally, the desired angular velocities of the right and left wheels are respectively derived as follows:

$$\omega_{r,d}(t_k) = \left[2v_d(t_k) + \omega_d(t_k)d\right]/(2r)$$
$$\omega_{l,d}(t_k) = \left[2v_d(t_k) - \omega_d(t_k)d\right]/(2r). \quad (13)$$

In summary, according to the assigned task two corresponding desired angular velocities of the right and left wheels are obtained. Then the fuzzy decentralized variable structure control (e.g., [8], [9]) is applied to make the angular velocities of the right and left wheels track the desired values.

Due to the feature of house architecture, the consumption of energy and the ease of path planning, a set of trajectory of piecewise-lines is applied for the path planning. The strategy for tracking the trajectory of piecewise-lines includes the following three modes (see Fig. 12): (i) approach mode, (ii) fine-tune mode, and (iii) inertia-navigation mode. As the DMR is in the approach mode (e.g., $|e(t_k)| > e_1$, where $e_1 = 20cm$), the strategy forces the DMR to approach the desired trajectory as fast as it can. It implies that in this mode the quantity of trajectory tracking is more important as compared with the quality of that. As the DMR is in the fine-tune mode (e.g., $e_1 \geq |e(t_k)| > e_2$, where $e_2 = 7.5cm$), the strategy adjusts the motion of the DMR to approach the desired trajectory as close as it can. The detail of the fine-tune mode is shown in Fig. 13. The DMR first turns an angle $\theta_d(t_k)$, travels with a desired translation velocity for the time interval $\Delta\tau = e(t_k)/\left[v_d(t_k)\sin(\theta_d(t_k))\right]$, then turns a negative value of the original angle, i.e., $-\theta_d(t_k)$. It indicates that the quality of trajectory tracking is most important in this mode. As the DMR is in the inertia-navigation mode (e.g., $|e(t_k)| \leq e_2$), the strategy

does not give any command to the DMR so that the energy consumption of the DMR is reduced under the acceptable tracking performance. In this final stage, the energy consumption for the DMR is more important. In summary, the proposed strategy for the trajectory tracking of piecewise-lines is a promising method for the navigation of all kinds of mobile robot.

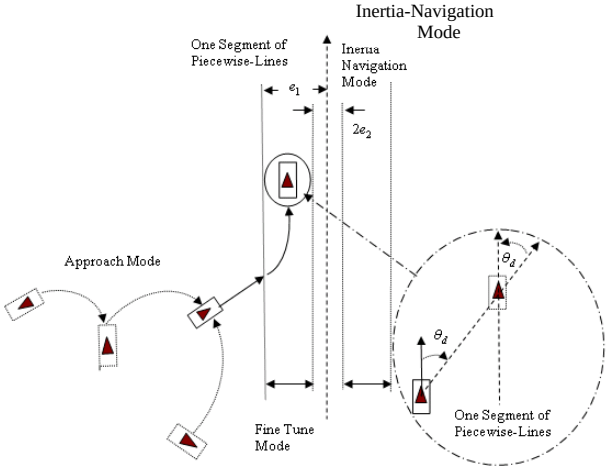

Fig. 12 Strategy for the trajectory tracking of piecewise-lines.

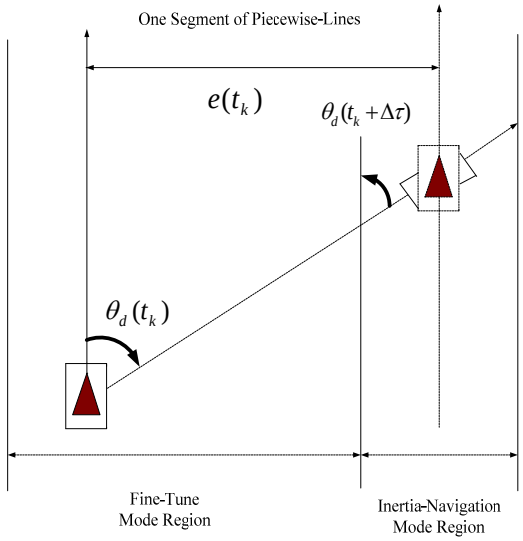

Fig. 13. Illustration of fine-tune mode.

V. Experiments and Discussions

5.1 Experimental Preliminaries

A. Posture estimation

The width of the overlap between the ends of the extreme areas of AEVS1 and 2 is about 24*cm*. The centerline of the overlap is set as the control authority for the two AEVS. The higher authority is in charge of the DMR. From our investigation, large estimation error only occurs in the peripheries of visible areas. The proposed modeling via MNN is simple, systematic, and effective. The average modeling error is 2*cm* (see Tables 2 and 3). In general, the large modeling error occurs in the periphery of visible region. Although the aforementioned calibration is based on static camera, the corresponding dynamic performance will be evaluated by five categories of experiments (i.e., Figs.14~21). According to the restriction of the grabbing frequency for an AEVS, the sampling time for the image processing and trajectory planning is set as 200*ms*. On the other hand, the sampling time (or control cycle time) for the DMR is only 10*ms*.

It is assumed that the dimension of the obstacle is not too large to hind the sight of AEVS. Fortunately, the AEVS is on the ceiling and its field of view is adjustable. The strategy for the obstacle avoidance can be found in (e.g., [8], [9]). In the beginning, a sequence of images grabbed by the two AEVS is obtained to judge whether obstacles are present in the visible area (or DAEVS space). If obstacles exist, the corresponding positions are applied for the trajectory planning to avoid these obstacles (see, Figs. 18~21).

B. Search of DMR or obstacle

If a DMR is initially not found inside the visible window of AEVS1 or 2, a search is needed. In the beginning, two labels at the origin and $(0, 640)cm$ of the world coordinate are found by the AEVS1, 2. Next, they are respectively set as the image centers of the AEVS1, 2. After this initialization, the whole areas are searched by AEVS1, 2 to find out whether the obstacles exist or not. If an obstacle exists, the position is recorded so that the obstacle avoidance is executed for the DMR in the neighborhood of the obstacle (e.g., Fig. 3). Sequentially, AEVS1, 2 simultaneously search the DMR in a butterfly manner (see [9]). Because the initial position of the AEVS1 or 2 is in the center of the monitoring area, the center of image plane is first assigned as the center of search. If the first search via the butterfly way (i.e., $r_{search} = r_0$) does not find the DMR, then a larger distance $r_{search} = r_0 + \Delta r$, where Δr denotes a suitable increment radius, is used for the next search until the maximum radius for AEVS1 or 2 is reached.

5.2 Experimental Results

A set of piecewise-lines to be tracked is made up by five straight line segments (i.e., the dash lines in Figs. 14~21). In addition, the central positions of two static obstacles with diameter 12*cm* are $(X, Y) = (128.5, 203.2)$ and $(-81, 438.4)cm$. The corresponding responses of four categories are shown in Figs. 14~21, where the symbols ■ and ★ are respectively start point and goal point. The processing time for Figs. 14~21 is about 63 second. The reference command of the translation velocity in the vicinity of the overlapped region and the obstacle avoidance is reduced to 25.*cm/s* so that the chance of discontinuity is minimized. To demonstrate the robust performance, the same experiment of Fig. 20 except that two extra sets of fluorescent lamp are lighted in the vicinity of the DAEVS is shown in Fig. 21. Generally, the performance of this project is satisfactory. However, the response in the vicinity of the overlap region (e.g., $270 < Y < 320cm$) is often a little inferior due to the discontinuity and poor quality of the image system. Because almost no minimum turning radius for a DMR exists, the tracking performance in the trajectory of the third segment still acceptable. This is one of the differences as compared with the previous papers (e.g., [8], [9]). Although a set of line segments to be tracked is

in the periphery of the DAEVS, exhibiting poor quality for posture estimation [22], [23], [25], the performance shown in Figs. 14~21 confirm the superiority of the control system. The limitation of the DMR's translation velocity is determined by the bandwidth and window size of AEVS1 or 2, the image processing time, and the computation time of the FDVSC. Based on a similar analysis of [22], the upper bound of the DMR's translation velocity in the vertical optical axis of the AEVS 1 or 2 is approximately estimated as 6.4 *m/s*, which is much greater than the translation velocity 35*cm/s*. Hence, there is no worry for the escape of the DMR from the field of view of the AEVS 1 or 2 once it is locked (or tracked). If the height of the landmarks for the DMR and the obstacle is much different, the output of the MNN model becomes three dimensions, i.e., (X_{Rw}, Y_{Rw}, Z_{Rw}). If the monitoring region increases, the number of AEVS should increase. That is, the setting here can be easily extended to more than two AEVSs.

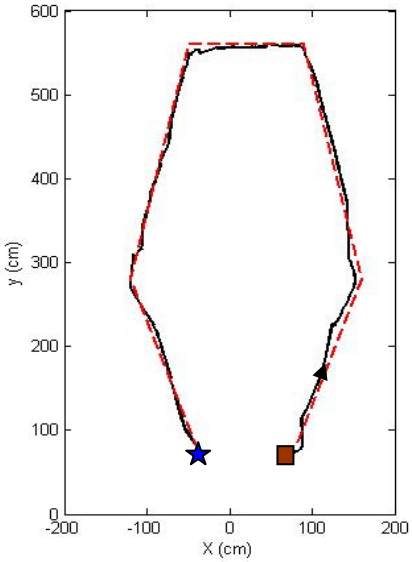

Fig. 14. Response of the DMR with an initial lock.

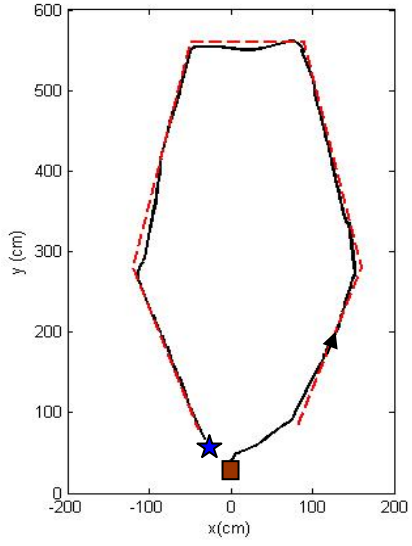

Fig. 15. Response of the DMR with an initial lock but different initial posture of the DMR.

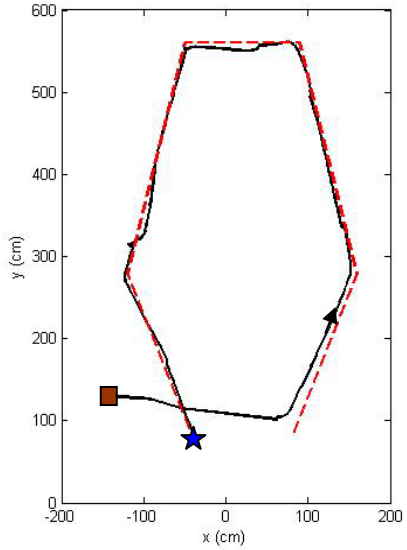

Fig. 16. Response of the DMR with an initial unlock.

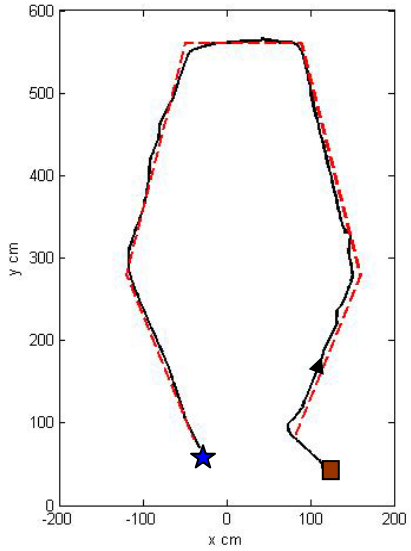

Fig. 17. Response of the DMR with an initial unlock and different initial posture as compared with Figure 16.

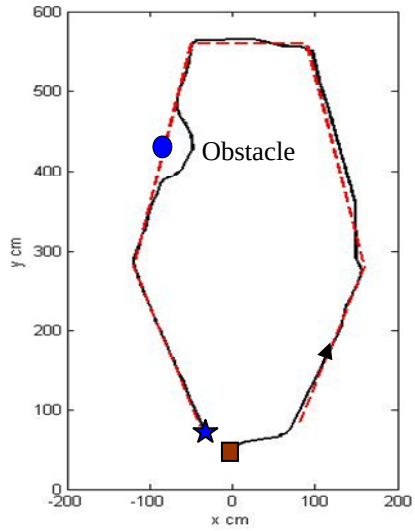

Fig. 18. Response of Figure 15 case with one obstacle.

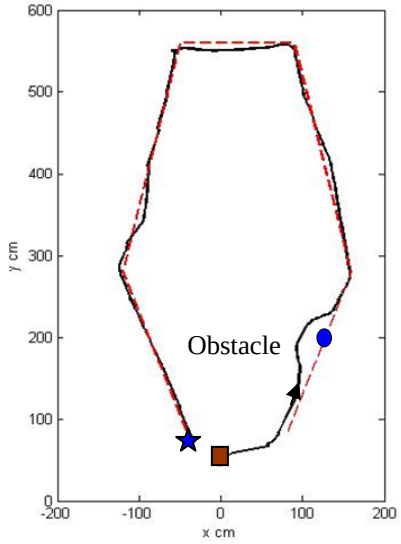

Fig. 19. Response of Figure 15 case with one obstacle different from Figure 18 case.

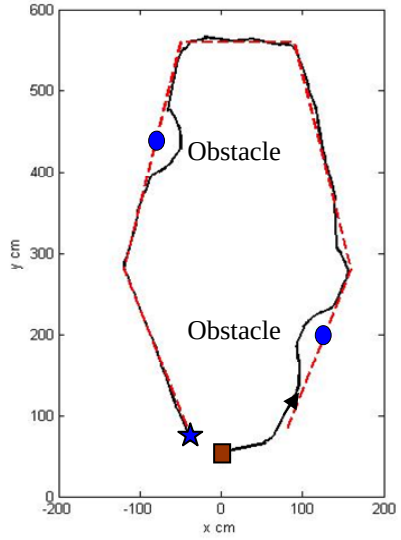

Fig. 20. Response of Figure 15 case with two obstacles.

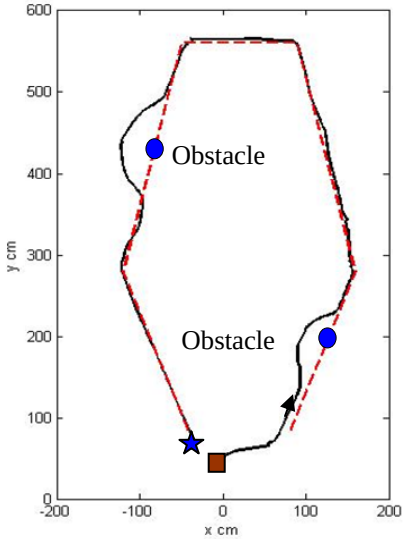

Fig. 21. Response of Figure 20 case with two obstacles and different lighting condition.

VI. Conclusions

A methodology for the trajectory tracking and obstacle avoidance of a DMR in a DAEVS using three FDVSCs is developed. The main contributions of this project are summarized as follows: (i) The manipulation of a DMR is different from that of a CLMR. The corresponding desired angular velocities of the right and left wheels for specific task are derived by the kinematics of a DMR. In addition, the response for the trajectory of piecewise-lines is better than that of a CLMR because almost no minimum turning radius for the DMR exists. This is the first difference as compared with the previous studies (e.g., [8], [9], [15], [20]). (ii) The second difference as compared with the previous studies is an active embedded vision system, possessing portable, computational, and wireless features. It is more suitable for the distributed sensor network system. (iii) From the viewpoint of the constraint of house architecture, the energy consumption of DMR, and the ease of path planning, a desired trajectory made up by a set of piecewise lines is addressed. Furthermore, the strategy for the trajectory tracking is designed and includes the following three modes: (a) approach mode, (b) fine-tune mode, and (c) inertia-navigation mode. Each mode has its main purpose. This is the third difference as compare with the previous papers. (iv) As compared with the classic modeling and the modeling of an ODVS, the proposed modeling using existing Matlab software is simple, systematic, and effective (e.g., average modeling error is 2*cm*). (v) The proposed visual tracking system is also robust to variant lighting conditions because two factors, i.e., color and shape, are employed to distinguish the DMR and obstacle from the background. Furthermore, the proposed setting can be easily extended when using more than 2 AEVSs or DMRs.

References

[1] T. Matsuyama and N. Ukita, "Real-time multitarget tracking by a cooperative distributed vision system," *Proceedings of the IEEE*, vol. 90, no. 7, pp. 1136-1150, 2002.

[2] T. Yamaguchi, E. Sato and Y. Takama, "Intelligent space and human centered robotics," *IEEE Trans. Ind. Electron.*, vol. 50, no. 5, pp. 881-889, Oct. 2003.

[3] J. H. Lee, K. Morioka, N. Ando and H. Hashimoto, "Cooperation of distributed intelligent sensors in intelligent environment," *IEEE/ASME Trans. Mechatronics*, vol. 9, no. 3, pp. 535-543, Sep. 2004.

[4] E. Menegatti, G. Cicirelli, C. Simionato, T. D'Orazio, and H. Ishigro, "Explicit knowledge distribution in an omnidirectional distributed vision system," *Proc. of Int. Conf. on Intell. Robots and Syst.*, Sendai, Japan, pp. 2743-2750, 2004.

[5] M. M. Trivedi, K. S. Huang and I. Mikic, "Dynamic context capture and distributed video arrays for intelligent space," *IEEE Trans. Syst. Man & Cyber, Part A*, vol. 35, no. 1, pp. 22-27, Jan. 2005.

[6] T. Sasaki and H. Hashimoto, "Human observation based mobile robot navigation in intelligent space," *IEEE Int. Conf. on Intelligent Robots and Systems*, Beijing, China, pp.1044-1049,. October 9 - 15, 2006.

[7] V. Lippiello, B. Siciliano and L. Villani, "Position-based visual servoing in industrial multirobot cells using a hybrid cameras configuration," *IEEE Trans. Robotics*, vol. 25, no. 1, pp. 73-86, Feb. 2007.

[8] C. L. Hwang and N. W. Chang, "Fuzzy decentralized sliding-mode control of car-like mobile robots in a distributed sensor-network space," *IEEE Trans. Fuzzy Syst.*, vol. 16, no. 1, pp. 97-109, Feb. 2008.

[9] C. L. Hwang and C. Y. Shih, "A distributed active vision network-space approach for trajectory tracking and obstacle avoidance of a wheeled robot," *IEEE Trans. Ind. Electronics*, vol. 56, no. 3, pp. 846-855, Mar. 2009.

[10] D. Lee and W. Chang, "Discrete-stature-based localization for indoor service robots," *IEEE Trans. Ind. Electron.*, vol. 53, no. 5, pp. 1737-1746, Oct. 2006.

[11] S. Han. H. S. Lim and J. M. Lee, "An efficient localizations scheme for a differential-driving mobile robot based on RFID system," *IEEE Trans. Ind. Electron.*, vol. 54, no. 6, pp. 3362-3369, Dec. 2007.

[12] S. Se, D. G. Lowe and J. J. Little, "Vision-based global localization and mapping for mobile robots," *IEEE Trans. Robot. & Automat.*, vol. 21, no. 3, pp. 364-375, Jun. 2005.

[13] D. Xu, L. Han, M. Tan and Y. F. Li, "Ceiling-based visual positioning for an indoor mobile robot with monocular vision" *IEEE Trans. Ind. Electron.*, vol. 56, no. 5, pp. 1617-1628, May 2009.

[14] J. Minguez and L. Montano, "Nearness diagram (ND) navigation: collision avoidance in troublesome scenarios," *IEEE Trans. Robot. & Automat.*, vol. 20, no. 1, pp. 45-59, Jan. 2004.

[15] T. H. S. Li, S. J. Chang, "Fuzzy target tracking control of autonomous mobile robots by using infrared sensors," *IEEE Trans. Fuzzy Syst.*, vol. 12, no. 4, pp. 491-501, Aug. 2004.

[16] A. A. Argyros, D. P. Tsakiris and C. Groyer, "Biomimetric centering behavior --- Mobile robots with panoramic sensors," *IEEE Robotics & Automat. Mag.*, pp. 21-31, Dec. 2004.

[17] E. Menegatti, A. Pretto, A. Scarpa, and E. Pagello, "Omni-directional vision scan matching for robot localization in dynamic environments," *IEEE Trans. Robotics*, vol. 22, no. 3, pp. 523-535, Jun. 2006.

[18] K. T. Song and J. C. Tai, "Dynamic calibration of pan-tilt-zoom cameras for traffic monitoring," *IEEE Trans. Syst. Man & Cybern., Pt. B*, vol. 36, no. 5, pp. 1091-1103, Oct. 2006.

[19] Y. Motai and A. Kosaka, "Hand-eye calibration applied to viewpoint selection for robotic vision," *Trans. Ind. Electron.*, vol. 55, no. 10, pp. 3731-3741, Oct. 2008.

[20] I. Baturone, F. J. Moreno-Velo, V. Blanco and J. Fervuz, "Design of embedded DSP-based fuzzy controllers for autonomous mobile robots," *IEEE Trans. Ind. Electron.*, vol. 55, no. 2, pp. 928-936, Feb. 2007.

[21] Y. S. Kung, "Design and implementation of a high-performance PMLSM drives using DSP chip," *IEEE Trans. Ind. Electronics*, vol. 55, no. 3, pp. 1341-1351, Mar. 2008.

[22] P. Vadakkepat, P. Lim, L. C. De Silva, L. Jing and L. L. Ling, "Multimodal approach to human-face detection and tracking," *IEEE Trans. Ind. Electron.*, vol. 55, no. 3, pp. 1385-1393, Mar. 2008.

[23] D. Xu, Y. F. Li, M. Tan and Y. Shen, "A new active visual for humanoid robots," *IEEE Trans. Syst. Man & Cyber., Part B*, vol. 38, no. 2, pp. 320-330, Apr. 2008.

[24] Y. Hu, W. Zhao and L. Wang, "Vision-based target tracking and collision avoidance for two autonomous fish," *IEEE Trans. Ind. Electronics*, vol. 56, no. 5, pp. 1401-1410, May 2009.

[25] Y. Han, "Imitation of human-eye motion --- how to fix gaze of an active vision system," *IEEE Trans. Syst. Mans & Cybern., Part A.*, vol. 37, no. 6, pp. 854-863, Nov. 2007.

Table 2. The real and estimation coordinates of AEVS1 via MNN.					
θ_x (degree)	θ_y (degree)	$X_{real}(cm)$	$Y_{real}(cm)$	$X_{estimation}(cm)$	$Y_{estimation}(cm)$
0	0	40	0	38.221	-1.09
0	0	40	20	37.499	18.687
0	0	40	40	38.623	41.374
0	0	60	0	60.767	2.547
0	0	60	20	59.033	20.245
0	0	60	40	58.425	39.507
0	7.5	0	0	0.623	0.781
0	7.5	0	20	1.169	17.922
0	7.5	0	40	0.846	39.524
0	7.5	0	60	1.67	58.45
0	7.5	0	80	1.493	81.339
0	7.5	-20	80	-18.258	79.848
0	7.5	-20	60	-19.007	59.158
0	7.5	-20	40	-21.324	40.39
0	7.5	-20	20	-19.335	20.839
0	7.5	-20	0	-22.739	2.981
0	15	0	80	0.825	80.116
0	15	0	100	0.236	99.341
0	15	0	120	1.518	119.814
0	15	-20	120	-17.45	120.602
0	15	-20	100	-18.531	99.946
0	15	-20	80	-21.078	81.101
0	15	-20	60	-20.508	58.921
0	15	-20	40	-21.368	41.261
0	45	80	220	77.374	216.785
0	45	80	240	78.503	239.079
0	45	80	260	78.909	260.657
0	45	80	280	81.978	280.401
0	45	80	300	80.649	301.298
0	45	80	320	82.029	323.781
0	45	80	340	81.072	352.088
-22.5	7.5	-40	40	-39.105	44.477
-22.5	7.5	-40	60	-38.223	61.204
-22.5	7.5	-40	80	-42.082	84.617

-22.5	7.5	-60	80	-61.931	91.318
-22.5	7.5	-60	60	-59.624	52.155
-22.5	7.5	-60	40	-59.389	36.041
-22.5	7.5	-60	20	-61.077	15.372
-22.5	7.5	-60	0	-62.926	-0.928
-22.5	22.5	20	80	18.66	79.59
-22.5	22.5	20	100	17.363	100.086
-22.5	22.5	20	120	17.63	124.069
-22.5	22.5	20	140	20.531	139.812
-22.5	22.5	20	160	22.284	161.066
-22.5	22.5	0	160	-2.133	160.424
-22.5	22.5	0	140	-0.592	141.169
-22.5	22.5	0	120	1.82	120.659
-45	30	-140	140	-141.885	137.213
-45	30	-140	120	-140.097	124.037
-45	30	-140	100	-140.493	99.897
-45	30	-140	80	-139.935	82.974
-45	30	-140	60	-139.848	58.78
-45	30	-160	80	-162.556	77.788
-45	30	-160	100	-160.855	96.291
-45	30	-160	120	-160.475	118.97
-45	30	-140	140	-141.885	137.213
-45	30	-140	120	-140.097	124.037
-45	45	-140	220	-137.283	218.523
-45	45	-140	200	-138.435	201.493
-45	45	-140	180	-137.646	179.898
-45	45	-140	160	-139.968	161.624
-45	45	-140	140	-139.206	141.39

Table 3. The real and estimation coordinates of AEVS2 via MNN.

θ_x (degree)	θ_y (degree)	$X_{real}(cm)$	$Y_{real}(cm)$	$X_{estimation}(cm)$	$Y_{estimation}(cm)$
0	7.5	20	600	20.788	599.471
0	7.5	20	580	19.685	577.672
0	7.5	40	580	42.54	577.231
0	7.5	40	600	42.425	598.75
0	7.5	40	620	40.954	617.27
0	7.5	40	640	40.102	639.077
45	7.5	0	580	0.114	578.874
45	7.5	0	600	1.591	600.076
45	7.5	0	620	3.49	617.107
45	7.5	0	640	1.715	638.435
45	7.5	0	660	2.796	654.214
45	7.5	20	640	20.277	638.772
0	15	-20	600	-21.487	603.057
0	15	-20	580	-20.244	581.103
0	15	-20	560	-21.277	560.14
0	15	-20	540	-22.324	540.45
0	15	-40	540	-39.675	540.004
0	15	-40	560	-38.724	560.022
45	15	20	560	22.626	562.61
45	15	0	540	0.967	545.113
45	15	0	560	-3.003	563.864
45	15	0	580	0.158	581.556
45	15	0	600	1.216	602.542
45	15	0	620	2.871	618.13
0	22.5	20	500	18.873	499.788
0	22.5	0	500	1.055	499.925
0	22.5	0	520	1.776	521.643
0	22.5	0	540	1.724	540.707
0	22.5	0	560	0.954	562.889
0	22.5	0	580	-0.486	581.504
45	22.5	-40	540	-40.735	539.487
45	22.5	-40	560	-39.552	561.367
45	22.5	-40	580	-39.218	579.003
45	22.5	-40	600	-39.264	600.22

45	22.5	-60	620	-59.652	619.313
45	22.5	-60	600	-60.586	600.593
0	30	20	480	19.361	480.556
0	30	20	460	21.524	460.062
0	30	20	440	19.149	439.147
0	30	0	440	2.873	440.528
0	30	0	460	0.835	459.506
0	30	0	480	0.979	481.154
45	30	-80	500	-80.929	498.24
45	30	-80	520	-79.728	518.766
45	30	-80	540	-80.109	538.809
45	30	-80	560	-81.288	559.592
45	30	-80	580	-81.333	579.211
45	30	-80	600	-79.335	600.292
0	37.5	0	480	-0.034	479.775
0	37.5	0	500	-0.372	498.834
0	37.5	0	520	-1.669	520.919
0	37.5	-20	520	-19.798	520.669
0	37.5	-20	500	-18.806	499.697
0	37.5	-20	480	-20.383	479.524
45	37.5	-100	440	-99.855	440.989
45	37.5	-120	420	-119.151	422.843
45	37.5	-120	440	-120.155	439.748
45	37.5	-120	460	-118.517	459.175
45	37.5	-120	480	-119.204	480.068
45	37.5	-120	500	-119.107	497.513
0	45	0	440	1.169	443.323
0	45	0	460	0.304	460.289
0	45	0	480	0.635	482.687

行政院國家科學委員會補助國內專家學者出席國際學術會議報告

97 年 6 月 10 日

報告人姓名	黃志良	服務機關及職稱	淡江大學電機系 教授
會議時間 會議地點	六月一至六日 中國/香港	本會核定補助文號	NSC-96-2221-E-032-012-MY2
會議名稱	（中文）IEEE 世界國會計算智慧會議 （英文）IEEE-WCCI2008		
發表論文題目	（中文）(1)應用模糊混合 H_2/H_∞ 最佳化設計分散控制於非線性連結動態延遲系統，(2) 應用模糊滑動輸入少於輸出的控制於具有自主動態平衡之電動腳踏車。 （英文）(1) Fuzzy Mixed H_2/H_∞ Optimized Design of Decentralized Control for Nonlinear Interconnected Dynamic Delay Systems, (2) Fuzzy Sliding-Mode Under-Actuated Control for Autonomous Dynamic Balance of an Electrical Bicycle.		

報告內容應包括下列各項：

一、參加會議經過

二、與會心得

三、考察參觀活動(無是項活動者省略)

四、建議

五、攜回資料名稱及內容

六、其他

出席 2008 年世界國會計算智慧會議(IEEE-WCCI2008)
心得報告

報告人：淡江大學 電機工程學系 黃　志　良

一. 參加會議經過

2008 年世界國會計算智慧會議(IEEE-WCCI2008)於中國香港召開，會議日期是從 6 月 1 日至 6 月 6 日止，共計六天。此次會議共有 548 篇論文投稿，每一篇論文均經過三位評審審查，通過率約 69%，亦即約 376 篇論文在此次會議發表，此次筆者所參與的會議場為模糊控制及系統。除了進行分組論文口頭及壁報發表外，大會現場並有相關書籍展示、產品展覽、及提供電子郵件服務。此次會議來自世界各國，約數百位專家學者參與，其中來自我國之與會人員約二十位，分別來自學術界、研究機構等。筆者亦在會中發表兩篇論文“(1)應用模糊混合 H_2/H_∞ 最佳化設計分散控制於非線性連結動態延遲系統，(2) 應用模糊滑動輸入少於輸出的控制於具有自主動態平衡之電動腳踏車。並與多位同領域的學者討論，使筆者獲益良多。

二. 與會心得

此次會議是一個大型的會議，主辦單位事先已將大會手冊預先寄給作者參考，且大會亦於事前透過網際網路將每位作者之論文發表時間告知，因此，筆者有相當充裕的時間安排所欲聆聽之論文發表。

筆者有幸獲得國科會之補助，前往中國香港參加 2008 年世界國會計算智慧會議(IEEE-WCCI2008)並發表論文，使筆者在各方面均有相當豐富之收穫。筆者近年來一直致力於非線性系統控制、強健適應控制、模糊類神經控制和建模及智慧型機器人之研究，因此與會期間，筆者曾就非線性系統控制、適應控制、及模糊控制等方面與與會之學者專家分享研究心得與經驗。並利用彼此討論機會和與會之學者專家建立友誼關係。

大會總共安排有口頭發表以及壁報論文，分為四個分組並行進行論文發表，每個人均可參加有興趣或較相近領域之論文發表。其中與筆者近年的研究較為相關的有如下之主題：(1) 非線性系統控制，(2) 模糊控制器設計，(3) 類神經控制及建模，(4) 機器人控制，(5) 適應控制系統。主講者對於未來的研究方向皆有詳細且完整的介紹，也有諸多建設性的建議及意見。

三. 建議

1. 承蒙國科會補助，謹此致謝。國內近來在學校的積極推動及補助下，使得有志研究的教師能藉由參與國際知名會議而獲得新知，也使得學校在舉辦國際性及區域性的研討會，有一良好的參考模式，如此爾後若能依照大會之作法稍加變通，當可使研討會辦的更精彩。
2. 同一個研討會可含蓋多個相關領域之論文，不同領域之研究方法有時可互通，並可提供與會學者深思，是否可擴展應用層面。
3. 廣邀與大會主題有關之廠商在會場設立攤位，此作法除可激勵學生了解應用層面提高興趣外，亦可讓與會的專家學者直接與廠商洽談合作之可能性或者訂購產品，以提升教學或研究內容。
4. 鼓勵研究生參與研討會並發表論文以展示自己的研究成果，如此不但可讓與會者了解各校之研究內容或水平，亦可讓學生有機會向各地之專家學者請益，以提升或改進自己的論文或水平。
5. 研討會設論文獎，以鼓勵優秀論文之作者，論文獎的獲獎者可由與會者投票產生或由專家評審表決產生。

四. 攜回資料名稱及內容

參加本次會議一共攜回下列資料：

1. 大會論文集光碟片一張、plenary/invited lectures 光碟片一張
2. 2008 IEEE World Congress on Computational Intelligence Programs & Abstracts。

五. 其他

香港位於中國的東南方，有四通八達的地鐵及公共巴士貫穿整個城市，是中國的特區，也是世界金融中心之一，筆者的旅館離會場約二十分鐘之路程，很容易掌控自己的行程；香港早晚溫差不大，白天溫度在攝氏 25~30 度左右，溼度適中。會議場所為香港會議展示中心，建築外觀為玻璃帷幕，非常雄偉壯觀，此地屬香港島市區，故相關公路路線之規劃非常完備，但因為處處都是現代化建築，故有些路在交通繁忙時，會出現塞車現象，故搭乘地鐵較方便，此次於會場中，有多位來自台灣的教授參加。畢竟，舉辦一個國際性研討會，不僅需在會議場地需做精心安排，會議所在地之城市及周遭環境亦需在人文及交通上具備可看性及便利性，才能吸引更多專家學者參與，這是值得我們借鏡之處。此處居民甚有禮貌，無種族歧視問題。